

Low-voltage electroosmotic pumping using porous anodic alumina membranes

Yu-Feng Chen · Ming-Chia Li · Yi-Hsin Hu ·
Wen-Jeng Chang · Chi-Chuan Wang

Received: 7 September 2007 / Accepted: 17 November 2007 / Published online: 6 December 2007
© Springer-Verlag 2007

Abstract This study demonstrated electroosmotic pumping with high flow rate per unit area at a rather low applied voltage by using alumina nano-porous membrane. The platinum mesh electrode is perpendicular to, and has direct contact with the nano-channel inlet for providing uniform electric field and for reducing the electric voltage drop in the reservoir. The measured flow rate versus electrolyte (KCl) concentration reveals two distinct characteristics. First, the flow rate is usually high at low concentrations (10^{-5} to 10^{-7} M) in which a maximum value occurs. Second, a remarkable drop of flow rate is seen when the concentration surpasses 10^{-4} M. The maximum flow rate achieved from this study is $0.09 \text{ mL/min V cm}^2$ and the energy transfer efficiency is 0.43% at an operation voltage of 20 V. The mesh electrodes with 33 wire spacing are capable of providing an uniform electric field, the nano-porous membrane with a low electrolyte concentration provides the environment for strong overlapping of electric double layer, in association with the thin alumina membrane, leading to a high flow rate at a rather low applied voltage (20–80 V). The flow rate is

comparable to the existing results whereas the corresponding operation voltage of this study is about one to two orders lower than most of the existing results.

Keywords Electroosmotic pumping · Pt mesh electrodes · Low voltage · Energy transfer efficiency · Nano-porous alumina membranes

1 Introduction

Electroosmotic flow (EOF) is developed through an applied electrical potential across a fine channel by manipulating the electrical double layer (EDL) between the electrolyte solution and dielectric channel wall (surface). The surface charge, zeta potential, ionic strength, applied electric strength, and the dielectric property of the mobile phase, characterize the magnitude of EOF. Over the past few years, EOF devices had shown promising aspects in a variety of applications including microflow pumping, microelectronics cooling, and bio-analytical applications (Laser and Santiago 2004; Chang and Yang 2007). However, some problems accompanied with conventional EOF pumping such as the need of a high supplied voltage (ranging from several hundred volts to several thousand volts) and low thermodynamic efficiency (<1%) may prohibit EO pumping from widespread exploitation. For the past several years, efforts toward augmentation of the thermodynamic efficiencies were reported, and efficiencies above 1% by applying high voltage [1.3% at 2 kV of Zeng et al. (2001); 5.6% at 1 kV of Reichmuth et al. (2003); 2.2% at 6 kV of Wang et al. (2006)] were reported. In addition to the low efficiency, high supplied voltage for the EO pumping may be even more severe. Firstly, the required high voltage may impede the applications of

Y.-F. Chen (✉) · C.-C. Wang
Energy and Environment Research Laboratories,
Industrial Technology Research Institute,
Hsinchu 310, Taiwan
e-mail: joanchen@itri.org.tw

M.-C. Li · W.-J. Chang
Department of Mechanical Engineering,
Feng Cha University, Taichung, Taiwan

Y.-H. Hu
Department of Chemical Engineering, National Yunlin
University of Science and Technology, Yunlin, Taiwan

integration with micro-electro-mechanical system (MEMS) and nano-electro-mechanical system (NEMS) (Zeng et al. 2001; Takamura et al. 2003; Yao et al. 2003; Brask et al. 2005). Furthermore, voltage drop, which was quantified by the ratio of applied voltage to the effective voltage ($V_{\text{app}}/V_{\text{eff}}$), is regarded as one of the major reasons responsible for the loss in efficiency (Yao and Santiago 2003). Hence, several studies had employed an electrode-free design within internal channel to avoid integration problem (McKnight et al. 2001; Dunphy Guzmàn et al. 2006) and to provide a roughly uniform electric field (Prakash et al. 2006; Yao et al. 2006).

According to previous studies (Yao et al. 2006; Vajandar et al. 2007), the utilization of porous media (Gan et al. 2000; Zeng et al. 2002; Tripp et al. 2004; Yao et al. 2003; Chen L et al. 2005a, b), or porous membrane (Chen W et al. 2005; Evans et al. 2006; Prakash et al. 2006; Yao et al. 2006; Vajandar et al. 2007) for EO pumping are quite beneficial for it have a high porosity, a low channel tortuosity, and a short channel length. Among the two, membrane-based EO pump is more attractive since it not only possesses the forgoing characteristics but can also be easily fabricated with a thinner membrane along with a high electric field. Recently, porous silicon membranes (Yao et al. 2006) and porous anodic alumina membranes (Chen W et al. 2005; Vajandar et al. 2007) have been demonstrated with high output flow rate capacity at a low-operation voltage (<100 V).

To achieve a maximum thermal efficiency is another requirement for EO pump development. Upon this requirement, several theoretical studies, such as Yao and Santiago (2003), Daiguji et al. (2004), and Min et al. (2004), indicated that the thermodynamic efficiency will reach a maximum when the channel size is comparable to the thickness of electric double layer (EDL), or even the EDL is strongly overlapped (van der Heyden et al. 2006). This is because the electrolyte becomes a unipolar liquid inside the channel. However, only very rare experimental studies (van der Heyden et al. 2006; Conlisk et al. 2007) had experimentally reported the feasibility of the concept concerning comparable EDL but none of them had demonstrated the concept of strongly EDL overlapped for EO pumping.

Motivated by the need to understand the EO flow in the nano-pipe whose electric double layer may be strongly overlapped, the objective of this study is to investigate the influence of nano-pore sizes (20, 100, and 200 nm) and electrolyte (KCl) concentrations (KCL, 10^{-7} to 10^{-3} M) subject to a low operating voltage on the performance of a EO pump. In addition, the characteristics of EO flow in a nano-pipe, such as conductance saturation, output flow rate, and energy transfer efficiency, are discussed.

2 Theory

Alumina is an amphoteric material whose surface electrical properties depend on the pH value of solution and its iso-electric point is at a pH value around 8. The pH value of present working fluid [deionized water (DI water) or aqueous KCl] is below 8; thus, alumina is protonated and has a positively charged surface (Chen W et al. 2005). When a voltage is applied across an alumina membrane, the excess counterions (OH^- of DI water or Cl^- of aqueous KCl) in the electric double layer (EDL) of the nano-pore will move and drag the liquid molecules with them by viscous force, giving rise to an electroosmotic flow (EOF). The alumina nano-porous membrane featuring high porosity, low tortuosity, and thin channel length is the key of the present electroosmotic pump (Vajandar et al. 2007). Due to the low tortuosity, each of the pores of the alumina membrane can be considered as an independent cylindrical channel.

2.1 Electroosmotic flow model

The equation of electroosmotic flow through a cylindrical pore can be expressed as (Levine et al. 1975):

$$u(r) = -\frac{1}{4\pi} (a^2 - r^2) \frac{dp}{dx} - \frac{\varepsilon}{4\pi\mu} [\zeta - \psi(r)]E \quad (1)$$

where dp/dx is the pressure gradient, a is the radius of circular tube, r is the distance from symmetry axial, ε is the permittivity of the electrolyte, ζ is the zeta potential, $\psi(r)$ is the radial potential due to the diffuse double layer, and E is the strength of the electric field.

The volume flow rate (Q) is given as (Levine et al. 1975):

$$Q = 2\pi \int_0^a ru(r)dr = -\frac{\pi a^4}{8\mu} \frac{dp}{dx} - \frac{\varepsilon \zeta a^2 (1 - G)E}{4\mu} \quad (2)$$

where

$$G = \frac{2}{\zeta a^2} \int_0^a r\psi(r)dr \quad (3)$$

which is the ratio of the mean electrostatic potential across the capillary to the ζ -potential.

In a symmetric electrolyte solution, $z^+ = -z^-$, the Poisson–Boltzmann (PB) equation can be expressed as

$$\frac{1}{r} \frac{d}{dr} \left(r \frac{d\psi}{dr} \right) = \frac{2n_0 z e}{\varepsilon} \sinh \left(\frac{ze\psi}{kT} \right) \quad (4)$$

where n_0 is the ionic number concentration, z is the absolute value of the ionic valence, e is the fundamental

charge of an electron, k is the Boltzmann constant, and T is the absolute temperature. Yao and Santiago (2003) solved Eq. 4 and compared the result of ψ with Debye–Hückel approximation. The Debye–Hückel approximation is valid when the electrical potential is small in comparison with the thermal energy of ions, i.e. $|ze\psi| < kT$ (surface potential $\psi \leq 25$ mV, Hunter 1981). Their result revealed a discrepancy between their direct numerical simulation and that by Debye–Hückel approximation, which was particularly pronounced for a/λ ratio of order 1 but virtually no difference when the ratios of a/λ was greater than 100 or less than 0.1. Here, λ is the Debye length (the reciprocal of the Debye–Hückel parameter, κ) and is calculated as

$$\lambda = \sqrt{\frac{\epsilon k_b T}{2n_0 z^2 e^2}} \tag{5}$$

In the present study, the corresponding a/λ values calculated from the nano-pore sizes with dilute KCl solution are generally between 0.01 and 10. Although the Debye–Hückel approximation may not be suitable for describing the physical phenomenon of the present case, the Debye–Hückel parameter ($\kappa = 1/\lambda$) is still used as an indicator for dimensionless pore size.

2.2 Thermodynamic efficiency of EO pump

The maximum flow rate (Q_{\max}) can be evaluated directly from Eq. 2 by setting the pressure gradient (dp/dx) to zero, while the maximum pressure or the maximum backpressure (P_{\max}) is obtained for the condition of zero net flow rate ($Q = 0$). The important characteristic of the EO pump is its energy transfer efficiency, E_{ff} , which is defined as the ratio of the useful work, ΔPQ , to the applied electrical work, VI (Zeng et al. 2001).

$$E_{\text{ff}} = \frac{\Delta PQ}{VI} = \frac{1}{4} \frac{P_{\max} Q_{\max}}{VI} \tag{6}$$

Where ΔP , Q , V , and I are the backpressure, output flow rate, applied electric potential, and measured current, respectively. The useful work (ΔPQ) is determined experimentally from flow rate versus backpressure (which is the pressure applied in the outlet of EO pump), and ΔPQ is equal to $\frac{1}{2} P_{\max} \times \frac{1}{2} Q_{\max}$.

2.3 Joule heating effect on electroosmotic flow

The temperature rise caused by the applied electric field is one of the major concerns of EO pumping. According to the energy balance in the channel, the following equation is used to describe the temperature rise (ΔT) over a period time Δt (Li 2004):

$$\Delta T = \frac{E^2 C \lambda_k \Delta t}{4.1868 C_v \rho} \tag{7}$$

where C is the ionic concentration (M), λ_k is the resistivity of KCl solution ($\text{m}^2 \Omega/\text{mol}$), C_v is the specific heat capacity [$\text{kcal}/(\text{kg } ^\circ\text{C})$], ρ is the liquid density [kg/m^3]. From Eq. 7, the temperature rise (ΔT) is proportional to the square of the applied electric field. For a given concentration, the upper limits of electric field should be examined to avoid the effect of the fluid properties by Joule heating (Li 2004).

3 Experimental setup

The schematic of the experimental setup is shown in Fig. 1. The fluidic system includes a holder which contains a nano-porous alumina membrane (Whatmann Inc.), a pair of Pt mesh electrodes, and a pair of Pt wire electrodes (Fig. 1). The Pt mesh electrodes are perpendicular to the flow direction and are placed fore and after the nano-porous alumina membrane. The fluid within the channel was driven by the provided electric field (power supplier, GW Instek GPR-11H30D), and the resultant flow rate and current were measured by an electronic balance meter (AND GF300) and a multi-meter (YOKOGAWA WT230) as depicted in Fig. 1.

Three different alumina membranes having nominal pore sizes of 20, 100, and 200 nm with a pore density of 10^{11} , 4×10^9 , and 10^9 per cm^2 were studied in the present experiment. The diameter and thickness of the membrane are 2.1 cm and 60 μm , respectively. The actual porosity of membranes with pore sizes of 20, 100, and 200 nm are calculated by the ratio of total pore area to total membrane area. The resultant porosity of membranes with 20, 100, and 200 nm pore size are all equal to 0.31. Thus the porosity effect could be neglected in the present study. The working fluid is deionized (DI) water in association with KCl electrolyte concentration ranging from 10^{-7} to 10^{-3} M. The Pt mesh electrodes were made by evaporating

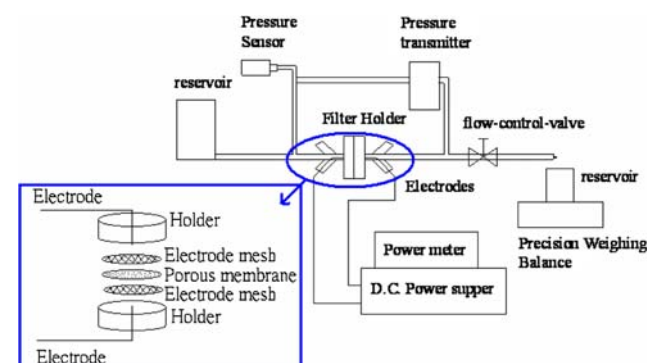


Fig. 1 The schematic of experimental setup

500 nm thick layer of Pt on the stainless mesh via an electron beam (E-gun). The stainless meshes from TWP Inc. with wire diameter and spacing of 20 and 20 μm , 30 and 33 μm , and 48 and 105 μm , are chosen for testing the effect of the electric field.

4 Results and discussion

4.1 Effect of mesh electrode spacing

The flow rate was measured and compared by using the following three spacing of meshes electrode, termed as E_A, E_B, and E_C. The corresponding wire diameter and spacing is 20 and 20 μm for E_A, 30 and 33 μm for E_B, and 48 and 105 μm for E_C. Figure 2 shows the comparison of flow rate versus voltage by using mesh electrodes E_A, E_B, and E_C. The measured flow rate for E_C is about 30–40% lower than those of E_A and E_B, indicating that the wire spacing of E_C (105 μm) is too sparse to provide enough uniform electric field for electroosmotic pumping. E_A (20 μm) and E_B (33 μm) are dense enough for providing a uniform electric field. The influence of wire diameter for the mesh electrode is rather small as seen in the figure. For effective pumping of the liquid flow, suitable mesh electrode wire spacing is needed. For the subsequent investigations, the E_B mesh electrode was chosen for further study.

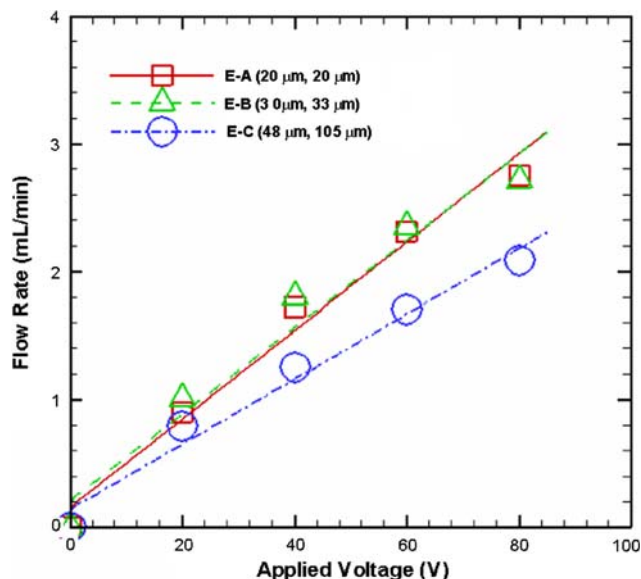


Fig. 2 The comparison flow rate versus voltage by using three electrode meshes spacing. E_A of wire diameter 20 μm and spacing of 20 μm ; E_B of wire diameter 30 μm and spacing of 33 μm , and E_C of wire diameter 48 μm and spacing of 105 μm (working fluid = DI water, pore size = 100 nm)

Accumulation flow rate versus time was recorded at a fixed applied voltage. After the voltage is applied, the flow rate (velocity) is increased from zero to a stable flow rate, and stays there for a sufficient time before it finally falls off due to deterioration. The deterioration is usually related to damage of electrode mesh or the bubble blockage inside the nano-pipe by water electrolysis. This period of time for stable flow rate is defined as the usable time (life span) of EO pump. The stable flow rate (velocity) in this process is defined as the output flow rate of a given voltage. The usable time versus applied voltage is plotted in Fig. 3. The usable time is more than 12 h of 20 V, and is less than 4 h of 80 V. It showed that the usable time of the present EO pump operated at a low applied voltage (~ 20 V) is longer than that at a high applied voltage (~ 60 –80 V). The lower operation voltage in a short membrane length subject to a high electric field is quite essential for a long period of electroosmotic pumping.

The thickness of the present porous alumina membrane is 60 μm . The electric field across the membrane ranges from 0.33 to 1.33 MV/m corresponding to a supplied voltage from 20 to 80 V. The effect of Joule heating on the temperature rise (ΔT) was less than 1°C for an applied voltage of 80 V (1.33 MV/m). For a typical ionic concentration $C = 1 \times 10^{-6}$ M, $\lambda_k = 149.79 \times 10^{-4}$ m²Ω/mol, $C_v = 1.0$ kcal/(kg °C) and $\rho = 1,000$ kg/m³, Eq. 7 can be expressed as $\Delta T = (3.58 \times 10^{-12})E^2 \Delta t$ (Li 2004). The corresponding temperature rise (Eq. 7) at an electric field 1.33 MV/m is near to 1.2°C, in which the period of time (Δt) was near to 0.2 s. Δt is calculated by the ratio of flow path (alumina membrane thickness = 60 μm) to the

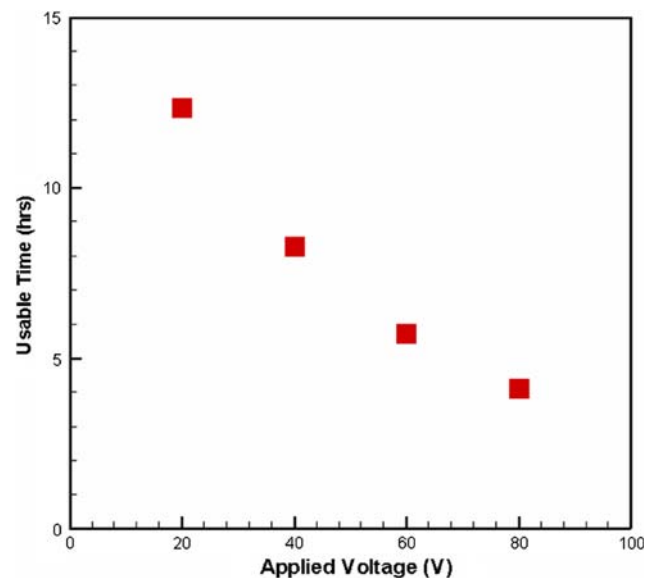


Fig. 3 The usable time versus applied voltage by using E_B (30 and 33 μm) Pt mesh electrode (working fluid = DI water, pore size = 100 nm)

measured average velocity. Notice that the resistivity (λ_k) of the working fluid also contributes to the Joule heating, and it is proportional to the electrolyte concentration. Tang et al. (2006) indicated that the Joule heating is negligible for a dilute concentration ($\leq 10^{-4}$ M). Li (2004) also indicated the upper limit of electric field of concentration $C = 1 \times 10^{-4}$ M is 1.4×10^2 MV/m, and under this limit, the Joule heating will not affect the fluid properties. The present study uses DI water with a low KCl electrolyte concentration ($\leq 10^{-3}$ M), and the electric field is less than 1.33 MV/m. In summary of the foregoing discussion, it is concluded that the Joule heating effect is negligible.

4.2 Effect of membrane pore size

Figure 4a presents the flow rate versus applied electric voltage by using porous alumina membranes having diameters of 20 nm, 100 nm, and 200 nm, respectively. As expected, the flow rate is increased with the size of pore diameter at a fixed voltage. However, one should notice that there is an upper limit of pore diameter. Based on the numerical analysis of Rice and Whitehead (1965), Levine et al. (1975), and Yao and Santiago (2003), the flow rate increased steadily with a/λ ratio in the range of 1–100, but it reaches a maximum value and stays unchanged when a/λ is larger than 100. This is because the pore size is too large compared to the thickness of EDL (λ); therefore, the generated EO pumping is too small to drag more liquid outside the diffuse layer. As a result, a low energy transfer efficiency is encountered. Note that there was no direct conduction of current through anodic membrane because the current–voltage characteristic with DI water shows a linear trend even at an applied voltage of 80 V (Fig. 4b), suggesting a good condition of electroosmotic pumping up to 80 V (electric field ~ 1.33 MV/m). The data obtained from this study is repeatable (actually all experiments have been repeated at least three times to ensure its repeatability). The fluctuation of flow rate, backpressure, and current were reflected by the error bar. The linear regression was also plotted in Figs. 4, and 5, and the R^2 value was greater than 0.95.

The characteristic of EO pump performance is shown in Fig. 5. For a given voltage, the backpressure (P_{max}) is proportional to the applied voltage (Fig. 5a), but it is inversely related to the channel size. Based on the Debye–Hückel approximation, the Debye Length (λ) from Eq. 5 of DI water is near 960 nm. Therefore, the influence of EDL overlapping is comparatively strong for a smaller channel like 20 nm, leading to higher ionic concentration and mobility inside the channel. This inevitably generates the highest backpressure for the smallest channel (20 nm). The energy transfer efficiency of three different pore sizes (20,

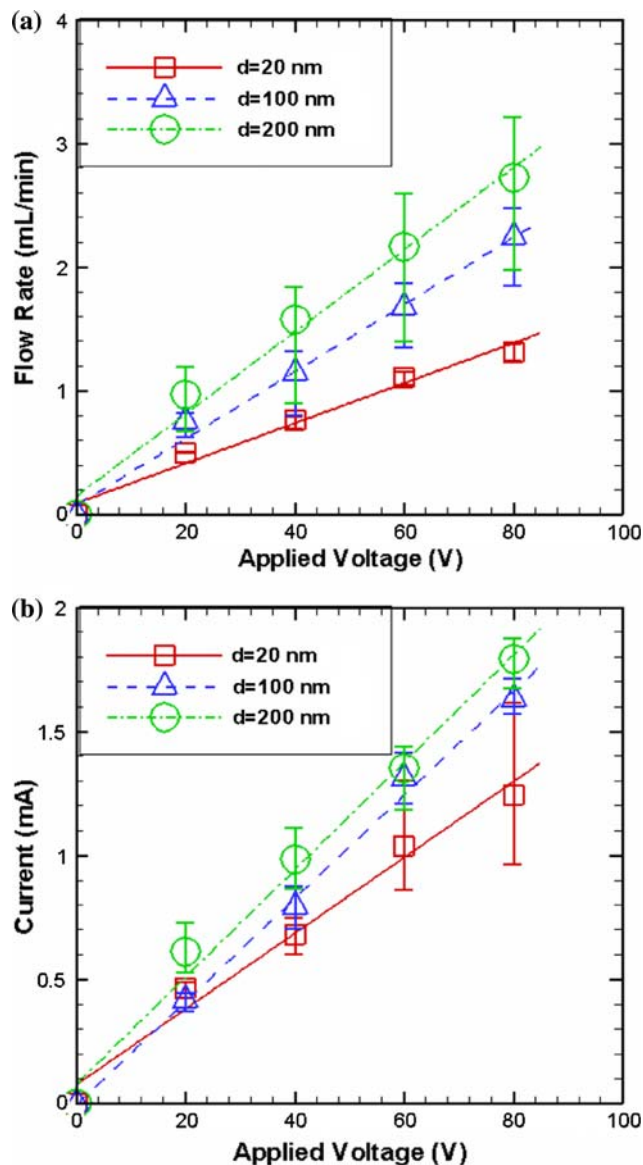


Fig. 4 a Flow rate versus electric voltage, and b current–voltage characteristic of 20, 100, and 200 nm porous diameter (buffer: DI water)

100, and 200 nm) with applied electric field is plotted in Fig. 5b. As seen in the figure, the maximum energy transfer efficiencies decreased with the rise of supplied voltage for all the pore diameters. The possible reason for the drop of efficiency is obviously related to bubble formation caused by water electrolysis at a sufficiently high electric field. The generated bubble will easily block the nano-channel and fail the whole system. For a low applied voltage (20 V), the maximum efficiencies for pore sizes of 20, 100, and 200 nm are approximately 0.28, 0.43, and 0.35%. From the result, there seems no direct linkage between efficiency and pore size. Part of the reasons may be attributed to the complicated composite interactions caused by the strong overlapping of electric double layer, bubble

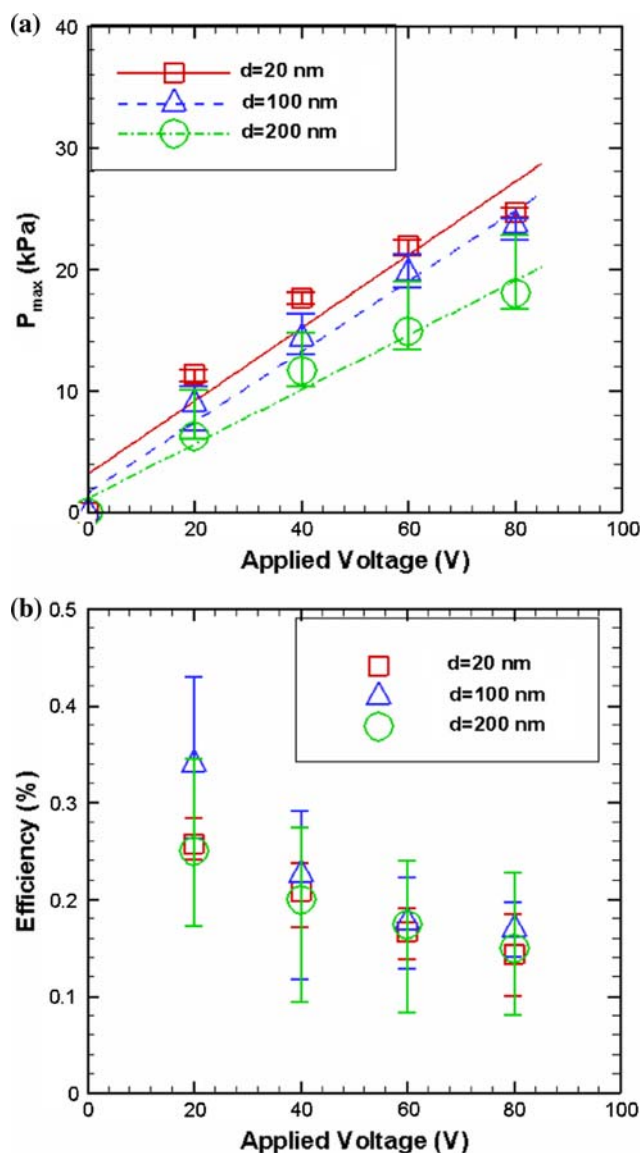


Fig. 5 **a** P_{max} , and **b** energy transfer efficiency versus electric voltage of pore diameter 20, 100, and 200 nm (buffer: DI water)

formation, or electroviscous in the low concentration electrolyte flow.

4.3 The effect of aqueous ionic concentration

The effect of ionic concentration plays an important role in EO pumping for it changes the thickness of the electric double layer. Figure 6a shows the relevant influence on the measured flow rate subject to an external electric field 20 V for three pore dimensions, yet the electrolyte solution is KCl with its range of concentration being varied from 10^{-7} to 10^{-3} M. As seen, regardless of the influence of pore diameter, the measured flow rate versus concentration reveals two distinct characteristics. Firstly, the flow rate is usually high in

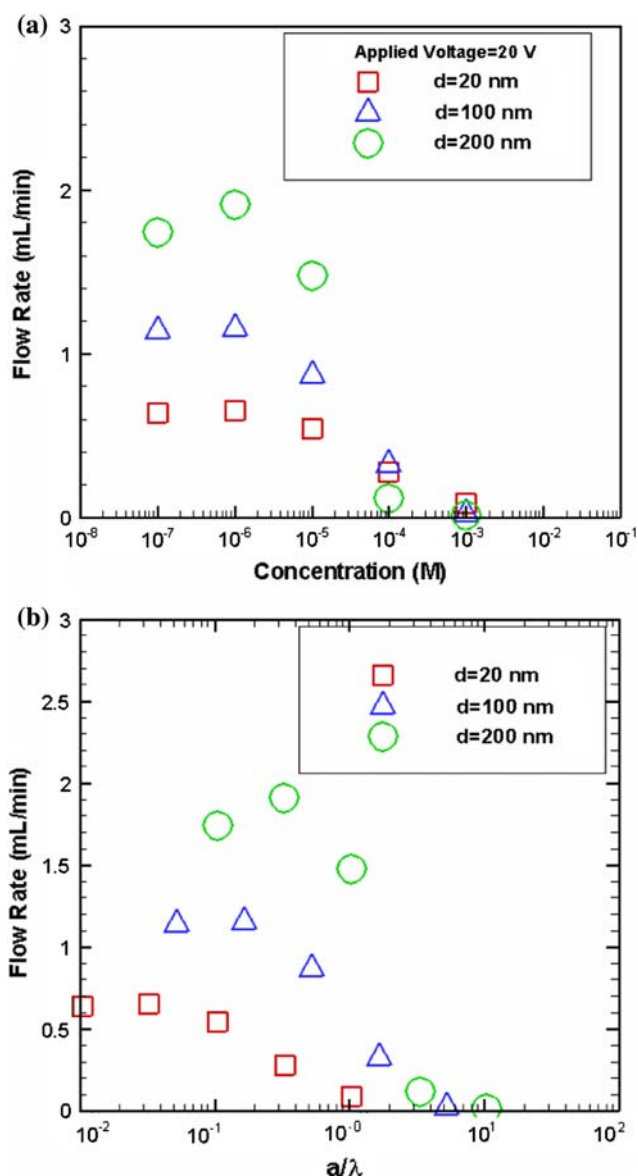


Fig. 6 **a** Flow rate versus KCl aqueous concentration; **b** the normalized flow rate versus nondimensional pore size $a^* (=a/\lambda)$ of 200, 100, and 20 nm of 20 V applied voltage

low concentrations (10^{-5} to 10^{-7} M) in which a maximum value occurs. Secondly, a remarkable drop of flow rate is seen when the concentration surpasses 10^{-4} M. According to the theoretical analysis of Eqs. 1–3, the flow rate is linearly related to zeta potential (ζ) and electric field (E). The reasons for the measured flow rate peaks at low concentration are mainly attributed to: (1) zeta potential (ζ) reaches a peak value at a certain concentration, (2) a rapid voltage drop in the nano-pore entrance, and (3) the thicker EDL of low electrolyte concentration. More detailed explanations about the foregoing reasons are in the following:

1. Zeta potential reaches a peak value at a certain concentration: The zeta potential of channel wall

surface is dependent on the ionic strength of electrolyte solution (Modi and Fuerstenau 1957; Hunter 1981). Modi and Fuerstenau (1957) had clearly showed the distinct behavior of a positively charged alumina surface pertaining to Cl^- and Na^+ . From their results, the zeta potential is generally increased with the concentration and peak at a certain concentration (near 2×10^{-6} M); then, it is decreased thereafter with further increase in concentration. A noticeable drop of the zeta potential is seen when the concentration is larger than 10^{-4} M. Huang and Yang (2007) also pointed out that the surface charge density is insensitive to the concentration in the low-salt regime. In summary to the forgoing discussions, the flow rate thus peaks at 10^{-5} to 10^{-7} M, and it drops significantly when the concentration is increased to 10^{-4} M in the present study (Fig. 6a). However, our result is opposite to the report by Vajandar et al. (2007), in which the electroosmotic pumping was operated using a borate buffer ($\text{Na}_2\text{B}_4\text{O}_7$) with pH ~ 9 and the flow rate was increased as concentration changing from 0.1 to 7.5 mM. They also mentioned that their results were opposite to the reports by Hunter (1981), Arulanandam and Li (2000), and Kirby and Hasselbrink (2004), but our results are in line with these previous studies. The complex adsorption process of ions is another reason in such a strongly overlapped case.

2. A rapid voltage drop in the nano-pore entrance: In this work, we found that the flow rate is high at a low concentration (Fig. 6a). From Eq. 2, the flow rate is proportional to the electric field (E). The low electric conductivity of low electrolyte concentration results in a rapid voltage drop at the nano-pore entrance and will lead to a high electric field (Conlisk et al. 2007). The high electric field at the nano-pore entrance becomes a dominant force by which a high flow rate occurring at the low concentration regime is encountered. Figure 7a, b shows the measured electrical current and electrical conductance ($S = I/E$) of the nanotube with a diameter of 20 nm. The electrical conductance is obtained by $S = I/E$, where I is the ionic current, and E is the parallel electric field. The measured electrical current and electrical conductance are increased linearly with the concentration (n) at high concentration region (10^{-3} to 10^{-5} M), and a further reduction of concentration from 10^{-5} to 10^{-7} results in a striking saturation regime in which both conductance and current were virtually independent of concentration. The present experimental results agree well with the conductance measurements reported by Karnik et al. (2005) and Stein et al. (2004). Based on the evidence of the conductance saturation at a low concentration, it is no surprise that the voltage drop caused by the nano-

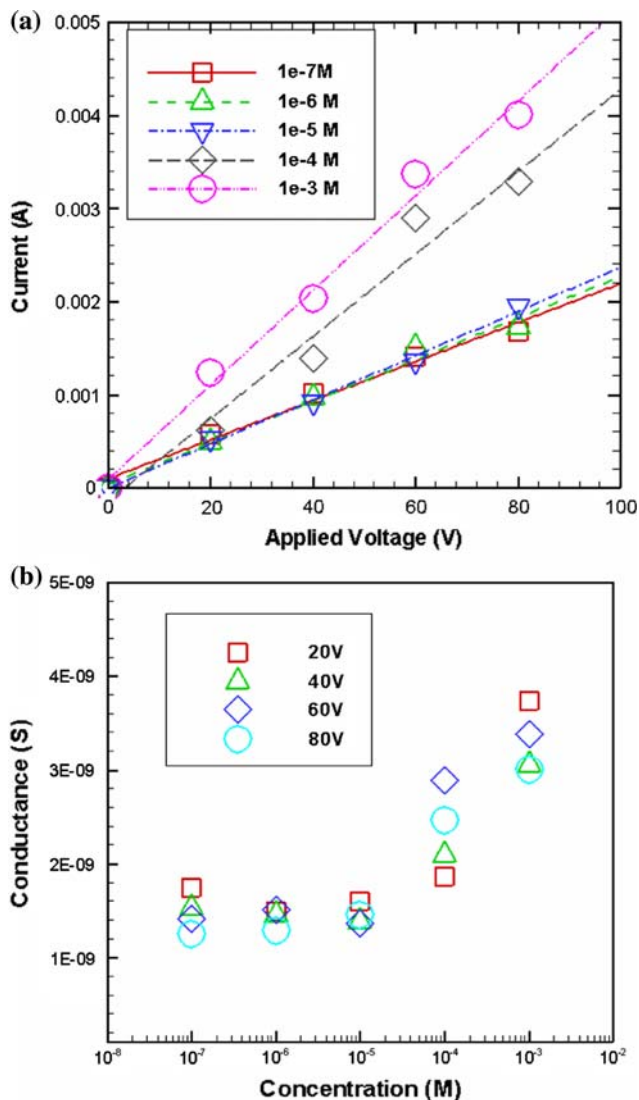


Fig. 7 a The electrical current versus applied voltage of KCl aqueous concentration ranging from 10^{-7} to 10^{-3} M; b electrical conductance versus KCl aqueous concentration of applied voltage ranging from 20 to 80 V (diameter = 20 nm)

pore entrance at a low concentration may lead to a larger flow rate.

3. The thicker EDL of low electrolyte concentration: From Eq. 5, the Debye length of KCl electrolyte is 960, 304, 96, 30, and 9.6 nm for a concentration of 10^{-7} , 10^{-6} , 10^{-5} , 10^{-4} , and 10^{-3} M, respectively. The permittivity of KCl aqueous is near 79. The corresponding a/λ values are between 0.01 and 10. Figure 6b plots the flow rate (Q_{max}) versus a/λ for pore diameters of 200 nm, 100 nm, and 20 nm at a supplied voltage of 20 V. The flow rate is comparatively high for $a/\lambda \leq 1$, but it drops considerably when $a/\lambda > 1$. The measured flow rate increases significantly when the electric double layer is overlapped at a given low electrolyte concentration. As shown by several

reports (Rice and Whitehead 1965; Levine et al. 1975; Yao and Santiago 2003; Vajandar et al. 2007), the flow rate is decreased in the range of $10 \geq a/\lambda \geq 1$. However, it is unclear when a/λ is less than 1. Recently van der Heyden et al. (2006) showed that the maximum energy conversion efficiency of electroviscous effect on pressure-driven liquid flow occurs at a low salt concentration in which the double-layer is strongly overlapped ($a/\lambda < 1$). Although, our results agree with their theoretical analysis, further studies are needed to quantify the influence of strongly overlapped double-layer on the resultant electroosmotic flow.

The forgoing discussions provide several clues for explanations of the measured results. However, it is difficult at this stage to identify which is the major effect on the resultant flow rate.

4.4 The performance of low-voltage EO pump

As mentioned earlier that one of the benefits of the present EO pump is a high porosity, a low channel tortuosity, and a short channel length accompanied with the alumina membrane. By applying a low operation voltage (20 V), it could provide a high electric field (0.33 MV/m) to drive fluid flow. Many previous studies had employed much higher voltage to provide a comparable electric field. For examples, 0.037 MV/m at 2 kV of Zeng et al. (2001), 1 MV/m at 1 kV of Chen and Santiago (2002), 0.05 MV/m at 5 kV of Chen L et al. (2005a), and 0.1 MV/m at 6 kV of Wang et al. (2006), and the like. However, it has been mentioned in Sect. 1 that high voltage may impede the applications of EO pumping. Hence, it would be interesting to make comparisons about this feature among existing literature. By including the present test results along with the previous comparisons made by Vajandar et al. (2007), the resultant flow rate versus applied voltage is shown in Fig. 8. The maximum flow rate achieved from this study is 0.09 mL/min V cm² at an operation voltage of 20 V, a pore diameter of 200 nm, and an electrolyte concentration of 10⁻⁶ M (Fig. 6a). The measured flow rate is comparable to the existing results whereas the corresponding operation voltage (20 V) of this study is about one to two orders lower than most of the existing results. The maximum thermodynamic efficiency is near 0.43% with an operation voltage of 20 V, a pore diameter of 100 nm, and electrolyte of DI water (Fig. 6a). A similar work by Yao et al. (2006), who used a spiral electrode with pore sizes ranging from 0.86 to 2.9 μ m, showed that the maximum flow rate is as high as 0.13 mL/min V cm² at a supplied voltage of 25 V but the maximum thermodynamic efficiency is only near 0.0003–0.005%. The main difference in efficiency is associated with the present test configurations being

capable of providing strongly overlapped EDL for effective electroosmotic pumping. For the EO pumping system, it not only needs to consider the output flow rate but also the power consumption (thermodynamic efficiency) of the system.

5 Conclusions

The present study has successfully demonstrated a low-voltage electroosmotic (EO) pumping system by using alumina nano-porous membrane with a Pt mesh electrode. Efforts are made towards a low operating voltage and a high energy transfer efficiency EO pump by manipulating nano-porous alumina membrane having three different pore sizes (20, 100, and 200 nm) and electrolyte concentration of KCl varying from 10⁻⁷ to 10⁻³ M. The maximum flow rate achieved is 0.09 mL/min V cm² and the maximum energy transfer efficiency is 0.43% at an operation voltage of 20 V. The flow rate peaks at a low concentration, where the electric double layer is strongly overlapped ($a/\lambda < 1$), is discussed. Some other major results from this study include:

1. The design of perpendicular mesh electrode can effectively reduce the electric voltage drop in the reservoir. The output flow rate is decreased as the Pt electrode mesh with sparse wire spacing (105 μ m), and suitable mesh wire spacing of 33 μ m is chosen for providing uniform electric field.

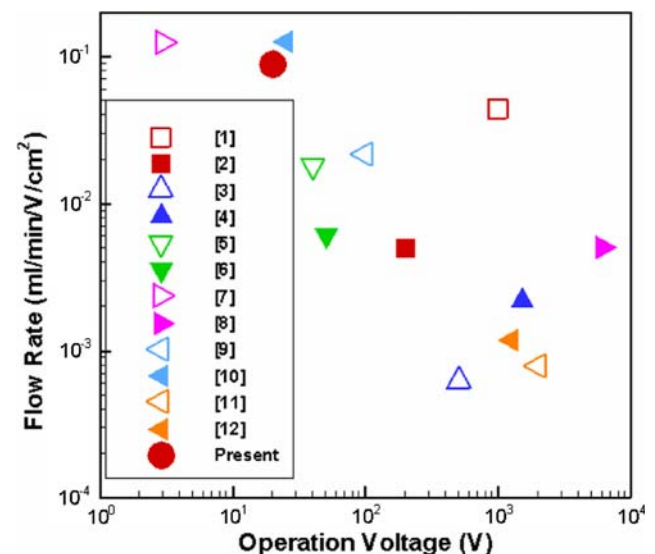


Fig. 8 Comparison of the flow rate between this study and other literatures listed: [1] Chen and Santiago (2002), [2] Jiang et al. (2002), [3] Gan et al. (2000), [4] Guenat et al. (2001), [5] McKnight et al. (2001), [6] Tripp et al. (2004), [7] Vajandar et al. (2007), [8] Wang et al. (2006), [9] Yao et al. (2003), [10] Yao et al. (2006), [11] Zeng et al. (2001), and [12] Zeng et al. (2002)

2. The flow rate is increased with pore diameter whereas the energy transfer efficiencies decreased with the rise of supplied voltage for these three different pore sizes. This is because bubble formation from water electrolysis at a high electric field may give rise to a blockage of the nano-channel.
3. The measured flow rate versus KCl electrolyte concentration reveals two distinct characteristics. Firstly, the flow rate is usually high in low concentration (10^{-5} to 10^{-7} M) in which a maximum value occurs. Secondly, a remarkable drop of flow rate is seen when the concentration surpasses 10^{-4} M. The flow rate peaks at a low concentration are attributed to (1) zeta potential (ζ), which reaches a peak value at a certain concentration; (2) a rapid voltage drop in the nanopore entrance; and (3) the thicker EDL of low electrolyte concentration. However, it is difficult at this stage to identify which is the major effect on the resultant flow rate.

Acknowledgments The authors highly appreciate the financial supports from the Department of Industry of the Ministry of Economic Affairs.

References

- Arulanandam S, Li D (2000) Liquid transport in rectangular microchannels by electroosmotic pumping. *Colloids Surf A* 161:89–102
- Brask A, Kutter JP, Bruus H (2005) Long-term stable electroosmotic pump with ion exchange membranes. *Lab Chip* 5:730–738
- Chang CC, Yang RJ (2007) Electrokinetic mixing in microfluidic systems. *Microfluid Nanofluid* 3:501–525
- Chen CH, Santiago JG (2002) A planar electroosmotic micropump. *J Microelectromech Syst* 11(6):672–683
- Chen L, Wang H, Ma J, Wang C, Guan Y (2005a) Fabrication and characterization of a multi-stage electroosmotic pump for liquid delivery. *Sens Actuators B* 104:117–123
- Chen L, Guan Y, Ma J, Luo G, Liu K (2005b) Application of a high-pressure electro-osmotic pump using nanometer silica in capillary liquid chromatography. *J Chromatogr A* 1064:19–24
- Chen W, Yuan J, Xia X (2005) Characteristic and manipulation of the electroosmotic flow in porous anodic alumina membranes. *Anal Chem* 77:8102–8108
- Conlisk AT, Kumar A, Rampersaud A (2007) Ionic and biomolecular transport in nanochannels. *Nanoscale Microscale Thermophys Eng* 11:177–199
- Daiguji H, Yang P, Szeri AJ, Majumdar A (2004) Electrochemomechanical energy conversion in nanofluidic channels. *Nano Lett* 4(12):2315–2321
- Dunphy Guzmàn KA, Karnik RN, Newman JS, Majumdar A (2006) Spatially controlled microfluidics using low-voltage electrokinetics. *J Microelectromech Syst* 15(1):237–245
- Evans CE, Noble RD, Koval CA (2006) A nonmechanical, membrane-based liquid pressurization system. *Ind Eng Chem Res* 45:472–475
- Gan WE, Yang L, He YZ, Zeng RH, Cervera ML, de la Guardia M (2000) Mechanism of porous core electroosmotic pump flow injection system and its application to determination of chromium(VI) in waste-water. *Talanta* 51:667–675
- Guenat OT, Ghiglione D, Morf WE, de Rooij NF (2001) Partial electroosmotic pumping in complex capillary systems Part 2: Fabrication and application of a micro total analysis system (μ TAS) suited for continuous volumetric nanotitrations. *Sens Actuators B* 72:273–282
- Huang KD, Yang RJ (2007) Electrokinetic behaviour of overlapped electric double layers in nanofluidic channels. *Nanotechnology* 18:115701(6pp)
- Hunter RJ (1981) *Zeta potential in colloid science: principles and applications*. Academic, London
- Jiang L, Mikkelsen J, Koo JM, Huber D, Yao S, Zhang L, Zhou P, Maveety JG, Prasher R, Santiago JG, Kenny TW, Goodson KE (2002) Closed-loop electroosmotic microchannel cooling system for VLSI circuits. *IEEE Trans Compon Packag Technol* 25(3):347–355
- Karnik R, Fan R, Yeu M, Li D, Yang P, Majumdar A (2005) Electrostatic control of ions and molecules in nanofluidic transistors. *Nano Lett* 5(5):943–948
- Kirby BJ, Hasselbrink EF (2004) Zeta potential of microfluidic substrates: 1. Theory, experimental techniques, and effects on separations. *Electrophoresis* 25:187–202
- Laser DJ, Santiago JG (2004) A review of micropumps. *J Micromech Microeng* 14:R35–R64
- Levine S, Marriott JR, Neale G, Epstein N (1975) Theory of electrokinetic flow in fine cylindrical capillaries at high zeta-potential. *J Colloid Interface Sci* 52(1):136–149
- Li D (2004) *Electrokinetic in microfluidics*. Elsevier/Academic, London
- McKnight TE, Culbertson CT, Jacobson SC, Ramsey JM (2001) Electroosmotically induced hydraulic pumping with integrated electrodes on microfluidic devices. *Anal Chem* 73:4045–4049
- Min JY, Hasselbrink EF, Kim SJ (2004) On the efficiency of electrokinetic pumping of liquids through nanoscale channels. *Sens Actuators B* 98:368–377
- Modi HJ, Fuerstenau DW (1957) Streaming potential studies on corundum in aqueous solutions of inorganic electrolytes. *J Phys Chem* 61:640
- Prakash P, Grissom MD, Rahn CD, Zydney AL (2006) Development of an electroosmotic pump for high performance actuation. *J Memb Sci* 286:153–160
- Reichmuth DS, Chirica GS, Kirby BJ (2003) Increasing the performance of high-pressure, high-efficiency electrokinetic micropumps using zwitterionic solute additives. *Sens Actuators B* 92: 37–43
- Rice CL, Whitehead R (1965) Electrokinetic flow in a narrow cylindrical capillary. *J Phys Chem* 69(11):4017–4024
- Stein D, Kruthof M, Dekker C (2004) Surface-charge-governed ion transport in nanofluidic channels. *Phys Rev Lett* 93(3):035901
- Takamura Y, Onoda H, Inokuchi H, Adachi S, Oki A, Horiike Y (2003) Low-voltage electroosmosis pump for stand-alone microfluidics devices. *Electrophoresis* 24:185–192
- Tang GY, Yan DG, Yang C, Gong HQ, Chai CJ, Lam YC (2006) Joule heating and its effects on electroosmotic flow in microfluidic channels. *J Phys Conf Ser* 34:925–930
- Tripp JA, Svec F, Fréchet JMJ, Zeng S, Mikkelsen JC, Santiago JG (2004) High-pressure electroosmotic pumps based on porous polymer monoliths. *Sens Actuators B* 99:66–73
- Vajandar SK, Xu D, Markov DA, Wikswo JP, Hofmeister W, Li D (2007) SiO₂-coated porous anodic alumina membranes for high flow rate electroosmotic pumping. *Nanotechnology* 18:275705
- van der Heyden FHH, Bonthuis DJ, Stein D, Meyer C, Dekker C (2006) Electrokinetic energy conversion efficiency in nanofluidic channels. *Nano Lett* 6(10):2232–2237
- Wang P, Chen Z, Chang HC (2006) A new electro-osmotic pump based on silica monoliths. *Sens Actuators B* 113:500–509

- Yao S, Santiago JG (2003) Porous glass electroosmotic pump: theory. *J Colloid Interface Sci* 268:133–142
- Yao S, Hertzog DE, Zeng S, Mikkelsen JC Jr, Santiago JG (2003) Porous glass electroosmotic pumps: design and experiments. *J Colloid Interface Sci* 268:143–153
- Yao S, Myers AM, Posner JD, Rose KA, Santiago JG (2006) Electroosmotic pumps fabricated from porous silicon membranes. *J Microelectromech Syst* 15(3):717–728
- Zeng SL, Chen CH, Mikkelsen JC, Santiago JG (2001) Fabrication and characterization of electroosmotic micropumps. *Sens Actuators B* 79:107–114
- Zeng S, Chen CH, Santiago JG, Chen JR, Zare RN, Tripp JA, Svec F, Fréchet JMJ (2002) Electroosmotic flow pumps with polymer frits. *Sens Actuators B* 82:209–212